Journal of Metals, Materials and Minerals, 36(1), e2346, 2026

Contributions of carbon content and cooling rate on phase transformations and mechanical properties of sintered Fe-1.5Cr-0.2Mo-*x*C alloys

Mantana YARUAN[1], Wantana KOETNIYOM[1,2], Thanyaporn YOTKAEW[3], Nattaya TOSANGTHUM[3], and Ruangdaj TONGSRI[3,*]

[1] *Department of Industrial Physics and Medical Instrumentation (IMI), Faculty of Applied Science, King Mongkut University of Technology North Bangkok, Bangkok 10800, Thailand.*
[2] *Lasers and Optics Research Center (LANDOS), King Mongkut's University of Technology North Bangkok, Bangkok 10800, Thailand*
[3] *Particulate Materials Processing Technology Laboratory (PMPT), Metal and Manufacturing Process Research Group (MMP), National Metal and Materials Technology Center,114 Phaholyothin Road, Khlong Nueng, Khlong Luang, Pathum Thani 12120, Thailand.*

***Corresponding author e-mail**: ruangdt@mtec.or.th

Received date:
3 March 2025
Revised date:
27 May 2025
Accepted date:
8 October 2025

Keywords:
Sintering;
Ferrite + carbide mixture;
Martensite-austenite constituent;
Mechanical property

Abstract

Microstructural development in sintered Fe-1.5Cr-0.2Mo-*x*C alloys, produced under different cooling rates of 0.1°C·s^{-1} and 5.4°C·s^{-1}, was investigated. It was found that, in slowly sintered Fe-1.5Cr-0.2Mo-*x*C alloys, the microstructure changed from hypoeutectoid to eutectoid and to hypereutectoid steel microstructural features with increasing carbon content. Under the fast-cooling rate of 5.4°C·s^{-1}, the microstructural change with respect to the increase of carbon content involved the competition between the formation of ferrite + carbide mixture and that of martensite-austenite constituent. The increase of tensile strength of slowly cooled sintered Fe-1.5Cr-0.2Mo-*x*C alloys with increasing carbon content was attributed to the increase of pearlite fraction, while the increase of tensile strength of fast-cooled sintered Fe-1.5Cr-0.2Mo-*x*C alloys was attributed to ferrite morphology change, the formation of ferrite + carbide mixture, and the formation of martensite-austenite constituent.

1. Introduction

Phase transformations, the causes of microstructural development in Fe-C steels, during slow continuous cooling or near equilibrium condition, can be simply explained by using the binary Fe-C phase diagram [1]. As given by Miyamoto *et al.* [2], phase transformation begins with the formation of ferrite as a proeutectoid phase and is followed by lamellar pearlite formation in hypoeutectoid Fe-C steels. In eutectoid steels, both ferrite and carbide phases transform cooperatively, resulting in lamellar pearlite formation. In hypereutectoid steels, carbide forms as a proeutectoid phase, followed by a eutectoid transformation resulting in lamellar pearlite.

Economic industrial steel productions rely on processes under continuous cooling [3-5]. In continuous cooling regimes, transformation types and products, and consequent mechanical properties in steels depend on both steel composition and cooling rate [6]. Both stable (known in the equilibrium Fe-C phase diagram) and metastable (not given in the equilibrium Fe-C phase diagram) phases, having strong influences on the mechanical properties of steels, can be formed under continuous cooling.

Most structural sintered alloys are also produced via continuous post-sintering cooling. Therefore, microstructures and mechanical properties of sintered alloys depend on both steel composition and cooling rate. However, the phase transformation products of modern metal powders cannot be simply predicted by using traditional metallurgical information. It was previously found that when the pre-alloyed Fe-0.5Mo-0.15Mn powder was employed, the sintered Fe-0.5Mo-0.15Mn-*x*C alloys showed unconventional eutectoid transformation products even under slow cooling with a rate of 0.1°C·s^{-1} [7]. By using pre-alloyed Fe-1.50Mo powder, the microstructural development in sintered Fe-1.50Mo-*x*C alloys (x = 0.30 wt% to 1.20 wt% with 0.15 increment) produced under cooling rates of 0.1°C·s^{-1} and 5.4°C·s^{-1} had eutectoid transformation products with microstructural features like those of upper bainite (UB) and inverse bainite (IB) [8].

According to Koetniyom *et al.* [9], carbon influences the microstructural development of Fe-1.5Mo-0.22B-C vacuum-sintered steel when produced at a cooling rate of 0.1°C·s^{-1}. In the absence of added carbon, the microstructure of this sintered steel consists of intergranular boride and polygonal ferrite grains. However, increasing the carbon content results in the formation of intergranular liquid phases and alters both the quantity and morphology of the eutectoid transformation products.

Conventional ferrite + M_3C lamellae or pearlite was hardly observed in sintered Fe-Mo-C alloys. The contributions of alloying with Mo and C elements and the cooling rate on microstructural developments in sintered Fe-Mo-C alloys are sufficiently comprehended.

However, there is less information regarding the combined contributions of alloying chromium (Cr) and C elements and cooling

rate on microstructural developments and consequent mechanical properties. The Cr-bearing metal powder, commercially known as Astaloy CrL powder according to Metal Powder Industries Federation (MPIF) Standard 35, FL-5208, with a composition of Fe-1.5Cr-0.2Mo, exhibits a relatively stable price trend compared to other alloying elements [10]. The Astaloy CrL powder was used to examine the relationship between microstructure and mechanical properties [11]. Sintered alloys, produced from Astaloy CrL powder modified with 1 wt% SiC or 3 wt% SiC and 0.6 wt% C additions and mechanical alloying, provided limited information on phase transformations due to low sintering temperature [12].

To deeply understand how the carbon content and cooling rate affect phase transformation and the subsequent mechanical properties of sintered Fe-1.5Cr-0.2Mo-xC alloys, varied C contents of 0.15 wt% to 1.20 wt% with 0.15 increment and varied cooling rates of 0.1°C·s^{-1} and 5.4°C·s^{-1} were experimentally conducted. To ensure homogenization of different Fe-1.5Cr-0.2Mo-*x*C austenite phases before transformations during post-sintering cooling, sintering was conducted at 1280°C for 45 min.

2. Experimental procedure

2.1 Material processing

The specimen preparation process began with mixing prealloyed Fe-1.5Cr-0.2Mo powder, Astaloy CrL grade of Hoganas (Sweden), 1 wt% zinc stearate, and varying graphite from 0.15 wt% to 1.20 wt% by 0.15 increment. By adding different graphite contents, different sintered Fe-1.5Cr-0.2Mo-xC alloys could be obtained. The nominal compositions of powder mixtures are shown in Table 1. After mixing, the powder mixtures were pressed into a dog bone shape as a tensile test bar (MPIF Standard 10), achieving a green density of 6.50 ± 0.05 g·cm^{-3}. Green compact specimens were sintered in a vacuum furnace (Schmetz, Germany) at 1280°C for 45 min. The specimens were divided into two groups to study how post-sintering cooling rate affects phase transformations, where the first group was cooled at a rate of 0.1°C·s^{-1} and the second one at a rate of 5.4°C·s^{-1}.

2.2 Materials characterization

The tensile specimens were cross-sectioned by abrasive cutting and hot compression mounted in phenolic resin for easier handling. According to ASTM E3-01 guidelines, specimens were first planarized to reduce the damage created by sectioning. The planar grinding step was accomplished by sequential grinding with silicon carbide (SiC) abrasive paper to obtain the desired surface finishes. The abrasive grinding procedure consists of 240 grit SiC paper followed by 400 grits, 600 grits, 800 grits, and 1200 grits, respectively. Polishing required three steps such as 6 μm, 3 μm, and 1 μm of diamond abrasive on nap polishing cloths until a smooth and scratch-free surface was achieved. The smooth surface of the samples was then dipped in 2% Nital etchant for 20 s before being washed with water and dried. The microstructure observation was done using optical microscopy (Olympus STM7 microscopes) and scanning electron microscopes (FE-SEM, Hitachi SU5000). The thermal effects associated with phase transformation in specimens were investigated using differential scanning calorimetry.

X-ray diffraction (XRD) investigation was done using a Rigaku TTRAX III apparatus equipped with a copper source (wavelength 1.5406 Å). The specimens were scanned in the angular two-theta range of 30° to 100° at a scan rate of 0.05°·s^{-1} and a step angle of 0.02°. Phase identification from XRD peaks was carried out by comparing them to established standards from the Joint Committee on Powder Diffraction Standards (JCPDS) card collection.

2.3 Mechanical properties

Hardness was measured using a Wilson Rockwell Scale B hardness tester, Model 574 Series. The 15 random points on the surface of three test samples were measured, and the average results were reported.

The tensile properties of the samples were thoroughly assessed using an Instron 8801 universal testing machine. This analysis strictly followed the widely recognized standard testing procedures outlined by ASTM E8. The tests were performed at a carefully controlled strain rate of 0.00174 s^{-1}. From the resulting stress-strain curve, we extracted detailed information regarding the ultimate tensile strength, which indicates the maximum stress the material can withstand before failure, the yield strength, which marks the point at which the material begins to deform plastically, and the elongation, which measures the material's ability to stretch before breaking.

Table 1. Nominal composition in mixed raw powder.

Alloy ID	Metal powder [wt%]	Nominal composition [wt%]			
		C	Mo	Cr	Fe
SC015C	99.85	0.15	0.20	1.50	Bal.
SC030C	99.70	0.30	0.20	1.50	Bal.
SC045C	99.55	0.45	0.20	1.49	Bal.
SC060C	99.40	0.60	0.20	1.49	Bal.
SC075C	99.25	0.75	0.20	1.49	Bal.
SC090C	99.10	0.90	0.20	1.49	Bal.
SC105C	98.95	1.05	0.20	1.48	Bal.
SC120C	98.80	1.20	0.20	1.48	Bal.
FC015C	99.85	0.15	0.20	1.50	Bal.
FC030C	99.70	0.30	0.20	1.50	Bal.
FC045C	99.55	0.45	0.20	1.49	Bal.
FC060C	99.40	0.60	0.20	1.49	Bal.
FC075C	99.25	0.75	0.20	1.49	Bal.
FC090C	99.10	0.90	0.20	1.49	Bal.
FC105C	98.95	1.05	0.20	1.48	Bal.
FC120C	98.80	1.20	0.20	1.48	Bal.

3. Results and discussion

3.1 Microstructures of sintered alloys

3.1.1 Sintered alloy with 0.15 wt% C addition

The slowly cooled sintered SC015C alloy showed a typical hypo-eutectoid steel microstructure consisting of large polygonal ferrite (PF) grains and eutectoid transformation zones (ETZs) consisting of pearlite nodules (Figure 1(a)). The average volume fractions of PF and ETZs were 87.87% and 12.13%, respectively. Under high SEM magnification, there were colonies of degenerate pearlite (DP) and lamellar pearlite (LP) in ETZs (Figure 1(b)). The XRD pattern of sintered SC015C alloy showed strong peaks of body-centered cubic (bcc) crystal structure of α-ferrite and weak peaks of the orthorhombic crystal structure of M_3C carbide (Figure 1(c)).

The microstructural feature of sintered SC015C alloy, consisting of PF grains and pearlite nodules, is typical in hypoeutectoid Fe-C steels. The coexistence of DP and LP structures in ETZs of this sintered alloy is a common phenomenon observed in steel with low carbon (C) content. The DP structure, with the same cementite crystallography and interlamellar spacing as those of LP but with broken or rod cementite particles, often forms in Fe-C steels with low C content [13].

The fast-cooled sintered FC015C alloy showed finer proeutectoid ferrite grains with ragged boundaries and ETZs (Figure 1(d)). Under high magnification, the ETZs comprised two different microstructural features, such as a ferrite + carbide (FC) mixture and undecomposed islands (Figure 1(e)). The FC mixture showed a multilayer structure with rows of discrete carbide particles on ferrite plate boundaries. However, the interlamellar spacing of the FC mixture was coarse and had varied values. The FC mixture could not be identified as DP but as upper bainite (UB). The UB definition and morphology, matching the microstructural feature of FC mixture in sintered FC015C alloy, were given in the literature [14]. The undecomposed islands were identified as martensite-austenite (MA) constituents. The XRD pattern of sintered FC015C alloy showed strong peaks of α-ferrite and very weak peak s of M_3C carbide (Figure 1(f)).

It is noted here that phase transformations in low-carbon (C) sintered alloys are strongly affected by the change in post-sintering cooling rate. The phase transformations in sintered SC015C alloy produced under the slow cooling rate of 0.1°C·s^{-1} include austenite to ferrite transformation, resulting in coarse equiaxed ferrite grain formation, and eutectoid transformation, resulting in DP and LP formations. With increasing cooling rate to 5.4°C·s^{-1}, phase transformations in sintered FC015C alloy include ferrite transformation resulting in fine irregular ferrite grain formation, bainite transformation resulting in UB formation, and martensite transformation resulting in MA constituent formation. The influence of cooling rate on microstructural development has been reported in several studies. The increase in cooling rate leads to a change in ferrite morphology from polygonal to acicular type [15].

3.1.2 Sintered alloy with 0.30 wt% C addition

The slowly cooled sintered SC030C alloy also showed a typical hypoeutectoid steel microstructure with a higher fraction of pearlite (Figure 2(a)). The average volume fractions of PF and pearlite were 60.49% and 39.51%, respectively. The pearlite structure showed dominant lamellar forms (Figure 2(b)). The XRD pattern of sintered SC030C alloy showed strong peaks of α-ferrite and weak peaks of M_3C carbide (Figure 2(c)).

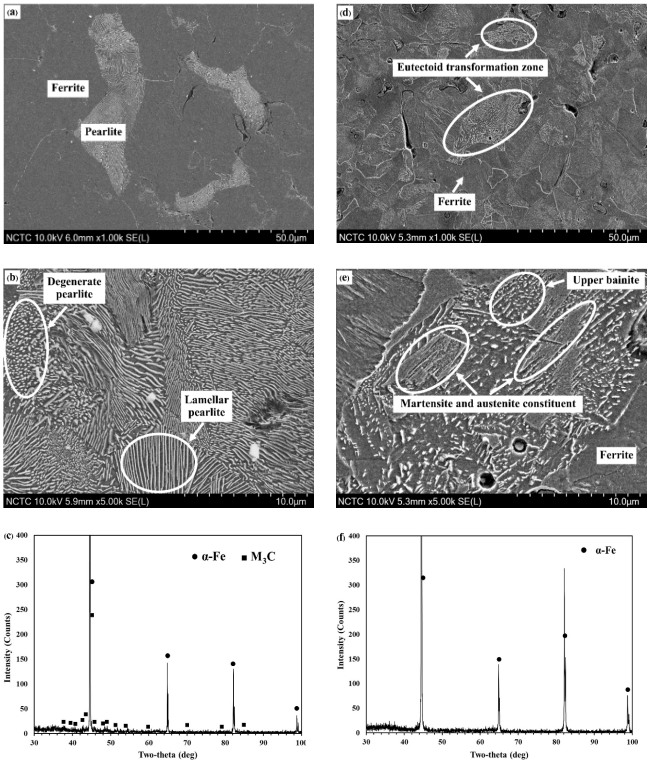

Figure 1. Characterization of sintered alloy with 0.15 wt% C addition, (a-c) sintered SC015C alloy, and (d-f) sintered FC015C alloy.

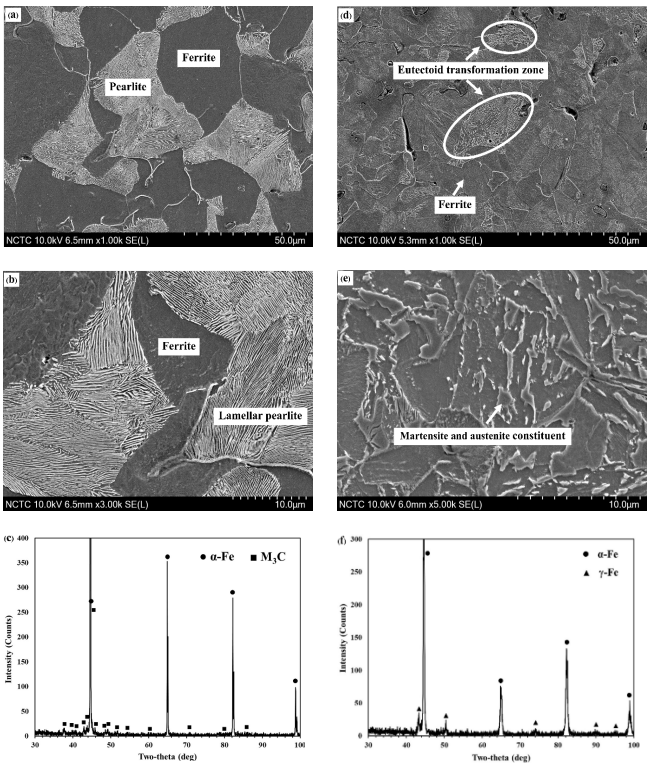

Figure 2. Characterization of sintered alloy with 0.30 wt% C addition, (a-c) sintered SC030C alloy, and (d-f) sintered FC030C alloy.

The fast-cooled sintered FC030C alloy showed an abrupt microstructural change, particularly ferrite change from large equiaxed grains to plate-shaped grains (Figure 2(d)). The MA constituents were clearly observed between plate-shaped ferrite grains (Figure 2(e)). A few carbide particles were observed on the ferrite plate boundaries. The XRD pattern of sintered FC030C alloy showed strong peaks of α-ferrite and moderate peaks of face-centered cubic (fcc) crystal structure of γ-austenite, whereas the peaks of M_3C appeared as XRD noises (Figure 2(f)).

The FC030C alloy microstructure consisting of ferrite plates and MA constituent islands on ferrite plate boundaries, as given in the SEM images (Figure 2(d,e), was defined as granular bainite (GB). According to the literature [16], the microstructure feature consisting of irregular ferrite with second phases distributed between the irregular ferrite grains is defined as GB, while that consisting of lath-like ferrite and carbon-enriched residual austenite or martensite (M/A) constituents on the lath boundaries is termed degenerate upper bainite (DUB).

When the fractions of MA constituents in sintered FC015C (Figure 1(d,e)) and FC030C (Figure 2(d,e)) alloys are compared, it is found that the MA constituent fraction in the latter sintered alloy is much higher. This indicates that at a cooling rate of 5.4°C·s^{-1}, carbon addition can promote MA constituent formation in sintered FC030C alloy. When the GB feature is considered, it can be implied that the increase of C content leads to the increase of stability of austenite islands remaining between irregular ferrite grains. Austenite islands are supposed to transform into MA islands during cooling down to room temperature. As given by Lan *et al.* [17], MA constituents were observed in low carbon steel isothermally treated at temperatures lower than or equal to 510°C.

Since sinter hardening combines the sintering process with a subsequent cooling rate sufficient to transform a significant portion of the material matrix into martensite [18], the microstructure of sintered FC030C alloy (Figure 2(d,e)) indicates that sinter hardening is successful under such sintered alloy composition and cooling rate of 5.4°C·s^{-1}.

3.1.3 Sintered alloy with 0.45 wt.% C addition

The slowly cooled sintered SC045C alloy also showed a typical hypoeutectoid steel microstructure with a pearlite fraction higher than that of ferrite (Figure 3(a)). The average volume fractions of PF and pearlite were 46.52% and 53.48%, respectively. The pearlite structure showed dominant lamellar forms (Figure 3(b)). The XRD pattern of sintered SC045C alloy showed strong peaks of α-ferrite and M_3C carbide (Figure 3(c)).

The fast-cooled sintered FC045C alloy showed ferrite plates and fine second phases on ferrite plate boundaries (Figure 3(d)). Under a high magnification SEM image, the second phases were revealed as short and long films of MA constituents and discrete carbide particles (Figure 3(e)). The XRD pattern of sintered FC045C alloy showed strong peaks of α-ferrite and weak peaks of γ-austenite and M_3C (Figure 3(f)).

The mixture of ferrite plates + short and long films of MA constituents on ferrite plate boundaries is defined as DUB as given in references [16], and the mixture of ferrite plates + discrete carbide particles is defined as UB, whose formation mechanism comprised at least two stages, the formation of parallel plates of ferrite and the transformation of the interspaces to a mixture of cementite and ferrite [19]. Thus, the microstructure of sintered FC045C alloy is characterized as a mixture of DUB and UB structures.

When the microstructures of sintered FC030C (Figure 2(d,e)) and FC045C (Figure 3(d,e)) alloys are compared, it is found that UB structure is hardly observed in the former alloy, whereas a high UB structure fraction is found in the latter alloy. This indicates that the decomposition of austenite bands between ferrite plates to form FC mixtures as the second stage of UB formation does occur in sintered FC045C alloy. The decomposition of austenite to FC mixture should be related to the increase of C content in this alloy, i.e., the increase of C content to 0.45 wt% C in sintered FC045C alloy leads to the increase of driving force for carbide precipitation in thin austenite bands between ferrite plates. The driving force for carbide precipitation is related to C content in a matrix [20].

3.1.4 Sintered alloy with 0.60 wt% C addition

The slowly cooled sintered SC060C alloy also exhibited a microstructure dominated by pearlite nodules with a few PF grains (Figure 4 (a)). The average volume fractions of PF and pearlite were 10.23% and 89.77%, respectively. In some regions, proeutectoid carbide particles were observed on prior austenite grain boundaries (Figure 4(b)). The XRD pattern of sintered SC060C alloy showed strong peaks of α-ferrite and moderate peaks of M_3C carbide (Figure 4(c)).

The fast-cooled sintered FC060C alloy showed a microstructure consisting of dominant UB structures and some MA islands (Figure 4(d,e)). The XRD pattern of sintered FC060C alloy showed strong peaks of α-ferrite, moderate peaks of M_3C, and weak peaks of γ-austenite (Figure 4(f)).

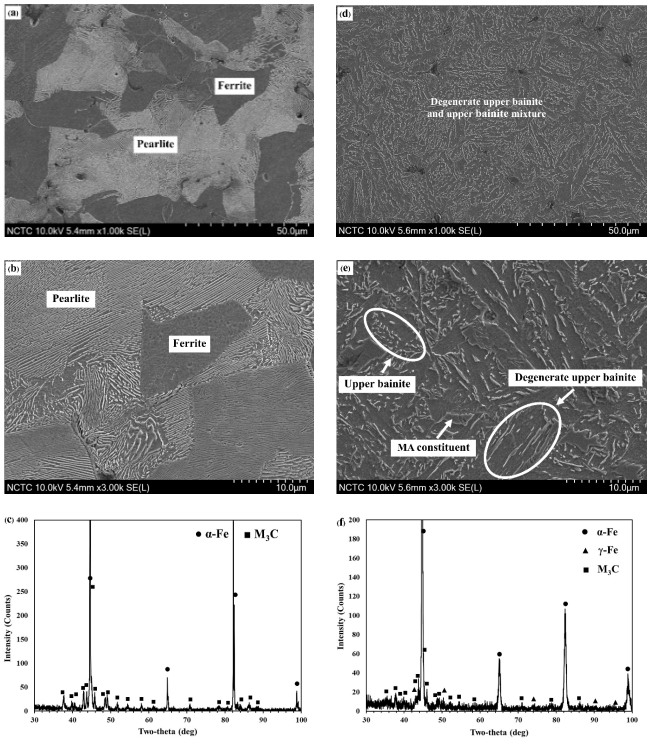

Figure 3. Characterization of sintered alloy with 0.45 wt% C addition, (a-c) sintered SC045C alloy, and (d-f) sintered FC045C alloy.

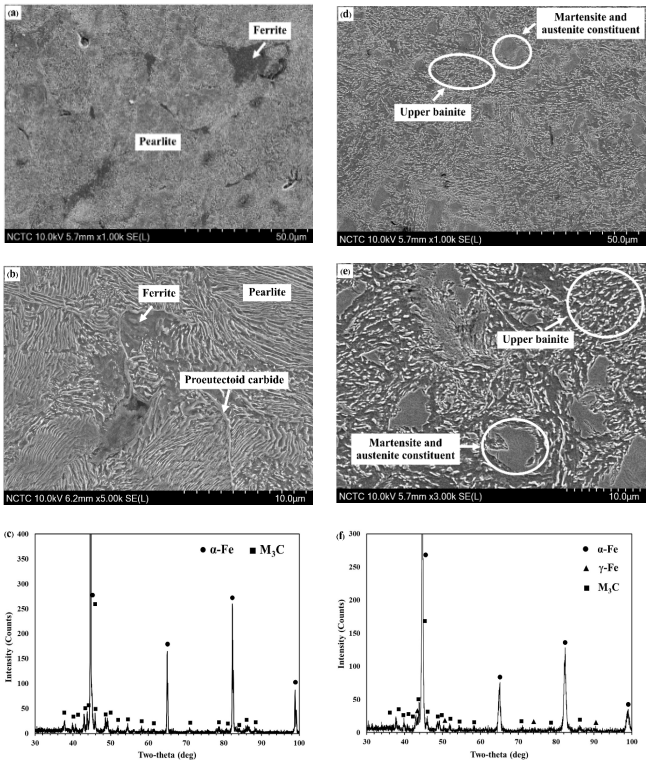

Figure 4. Characterization of sintered alloy with 0.60 wt% C addition, (a-c) sintered SC060C alloy, and (d-f) sintered FC060C alloy.

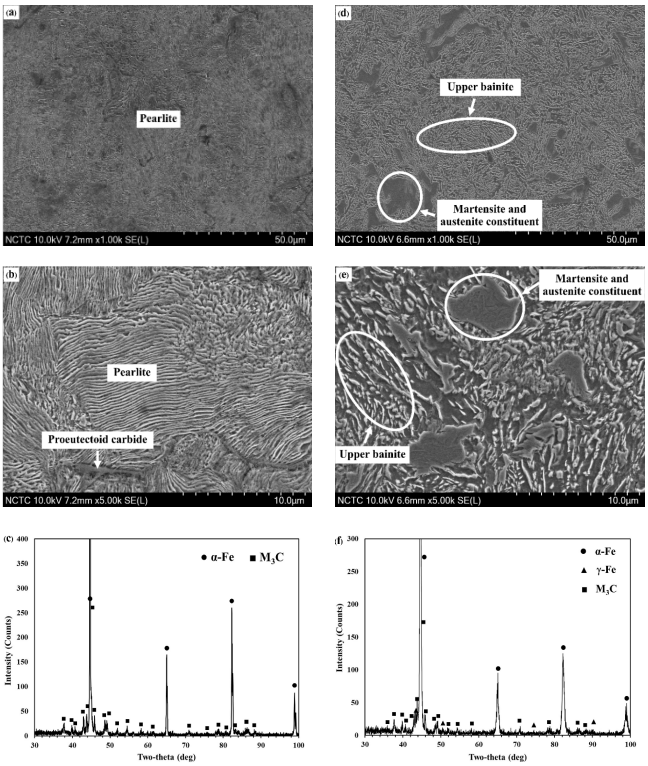

Figure 5. Characterization of sintered alloy with 0.75 wt% C addition, (a-c) sintered SC075C alloy, and (d-f) sintered FC075C alloy.

The domination of UB structures over MA islands in sintered FC060C alloy also confirms the influence of high C content on the increase of driving force for carbide precipitation in thin austenite bands between ferrite plates.

Zhao *et al.* [21] reported that "The formation of MA islands was claimed to be due to the partitioning of carbon during the transformation to acicular ferrite and the post transformation of carbon-enriched austenite". Later, it was confirmed by Moreno-Fabian [22] that "the MA formation occurred in two stages: carbon diffusion in austenite above the start of bainitic transformation (B_s) and carbon diffusion between bainitic ferrite and austenite at low temperatures"

3.1.5 Sintered alloy with 0.75 wt% C addition

The slowly cooled sintered SC075C alloy also showed a microstructure full of pearlite nodules (Figure 5(a)). In some regions, proeutectoid carbide particles were observed on prior austenite grain boundaries (Figure 5(b)). The XRD pattern of sintered SC075C alloy showed strong peaks of α-ferrite and strong peaks of M_3C carbide (Figure 5(c)).

The fast-cooled sintered FC075C alloy showed a microstructure consisting of dominant UB mixtures and some MA blocks (Figure 5 (d,e)). The XRD pattern of sintered FC060C alloy showed strong peaks of α-ferrite, moderate peaks of M_3C, and weak peaks of γ-austenite (Figure 5(f)).

3.1.6 Sintered alloy with 0.90 wt% C addition

The slowly cooled sintered SC090 C alloy also showed a microstructure full of pearlite nodules (Figure 6(a)). Thin proeutectoid carbide particles clearly highlighted prior austenite grain boundaries (Figure 6(b)). The XRD pattern of sintered SC090C alloy showed strong peaks of α-ferrite and M_3C carbide (Figure 6(c)).

The fast-cooled sintered FC090C alloy showed a microstructure consisting of FC mixtures and MA blocks with nearly equal fractions (Figure 6(d)). In most FC mixtures, the feature consisting of elongated spline carbide particles sheathed with ferrite and secondary discrete carbide particles was observed (Figure 6(e)). This FC mixture was identified as IB. The XRD pattern of sintered FC090C alloy showed strong peaks of α-ferrite and γ-austenite, whereas those of M_3C appeared as noise (Figure 6(f)).

Since IB forms below the pearlite transformation field, the highest temperature for IB transformation can be regarded as the lowest temperature for pearlite transformation [23]. The IB was previously reported as the eutectoid transformation products of hypereutectoid Fe-C steels isothermally heat-treated at a temperature range of 450°C to 700°C [24].

It is noted here that the formation of IB in sintered FC090C alloy is dependent on the driving force for the formation of Widmanstätten carbide particles as the leading phase in hypereutectoid steels, as given by Kannan *et al.* [23]. However, the experimental results show that the IB does not form in the slowly cooled sintered SC090C alloy, but it does form in the fast-cooled sintered FC090C alloy. The influence of cooling rate on IB formation in sintered hypereutectoid alloys needs explanation. In the past works, IB formed in hypereutectoid steels isothermally treated at temperatures below 500°C after austenitization for 10 min at 1373 K (1100°C) in argon [25]. Although the cooling rate from austenitization temperature to the isothermal heat treatment one was not given in the reference [25], it is assumed here that the austenite is preserved from austenitization temperature until reaching the isothermal heat treatment temperature, at which IB forms.

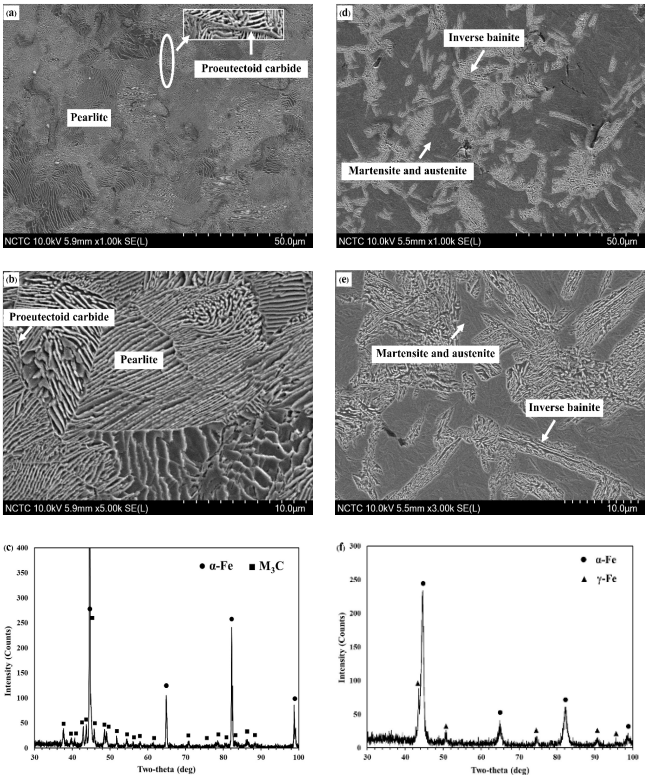

Figure 6. Characterization of sintered alloy with 0.90 wt% C addition, (a-c) sintered SC090 C alloy, and (d-f) sintered FC090 C alloy.

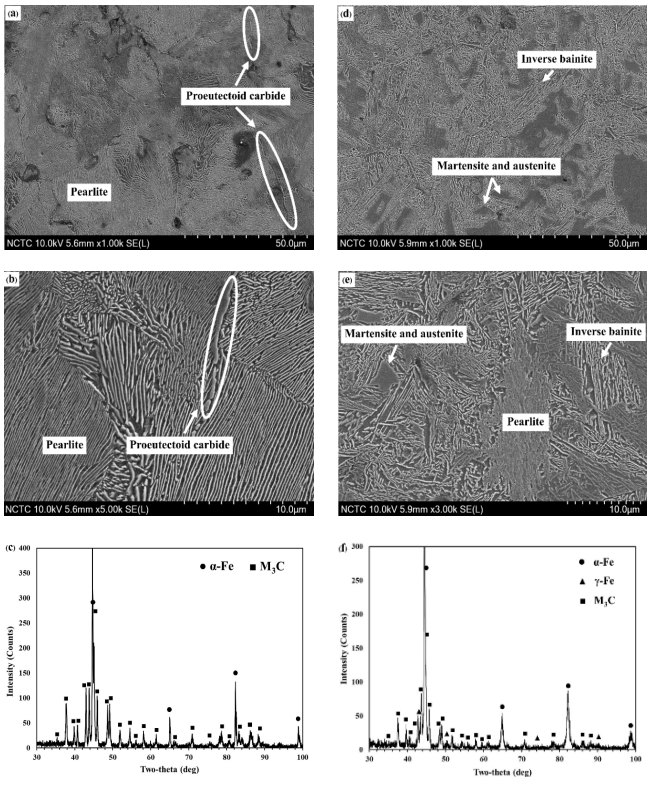

Figure 7. Characterization of sintered alloy with 1.05 wt% C addition, (a-c) sintered SC105C alloy, and (d-f) sintered FC105C alloy.

The microstructural feature consisting of IB units distributed in the MA matrix, as given in Figure 6(d,e), was also previously observed in some previous works. Few nodules of pearlite, bainite, and IB were found in the MA matrix of fast-cooled sintered 21Si09(c) steel [26].

3.1.7 Sintered alloy with 1.05 wt% C addition

The slowly cooled sintered SC105C alloy also showed a microstructure of fully pearlite nodules (Figure 7(a)). Thick proeutectoid carbide particles clearly highlighted prior austenite grain boundaries (Figure 7(b)). The XRD pattern of sintered SC105C alloy showed strong peaks of α-ferrite and M_3C carbide (Figure 7(c)).

The fast-cooled sintered FC105C alloy showed a microstructure consisting of dominant IB units and some MA blocks (Figure 7(d)). An acicular pearlite colony was also observed among inverse bainite structures (Figure 7(e)). The XRD pattern of sintered FC105 C alloy revealed strong peaks of α-ferrite and M_3C and weak peaks of γ-austenite (Figure 7(f)).

3.1.8 Sintered alloy with 1.20 wt% C addition

The slowly cooled sintered SC120C alloy also showed a microstructure full of pearlite nodules (Figure 8(a)). Thick proeutectoid carbide particles clearly highlighted prior austenite grain boundaries (Figure 8(b)). The XRD pattern of sintered SC120C alloy showed strong peaks of α-ferrite and M_3C carbide (Figure 8(c)).

The fast-cooled sintered FC120C alloy showed a microstructure consisting of a dominant IB structure and some MA blocks (Figure 8(d,e). Thick proeutectoid carbide particles clearly highlighted prior austenite grain boundaries. The XRD pattern of slowly cooled sintered SC120C showed strong peaks of α-ferrite and M_3C and weak peaks of γ-austenite (Figure 8(f)).

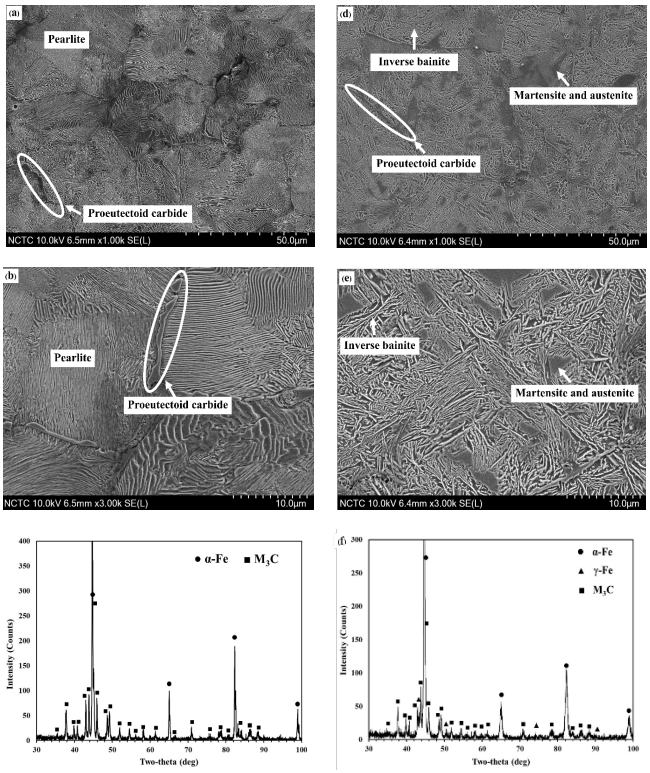

Figure 8. Characterization of sintered alloy with 1.20 wt.% C addition, (a-c) sintered SC120C alloy, and (d-f) sintered FC120C alloy.

3.2 Mechanical property

Tensile strength (Figure 9(a)), yield strength (Figure 9(b)), and hardness (Figure 9(d)) increased, whereas elongation (Figure 9(c)) decreased with increasing C content and cooling rate. All fast-cooled sintered alloys showed improved tensile strength, yield strength, and hardness values compared to those slowly cooled sintered alloys. In contrast, the elongation values in all fast-cooled sintered alloys were inferior to those of slowly cooled sintered alloys. The strength-ductility tradeoff dilemma existed in both slowly and fast-cooled sintered alloys.

In slowly cooled sintered alloys, tensile strength, yield strength, and hardness values increased with increasing C contents of up to 0.75 wt%. With C contents of > 0.75 wt%, tensile strength values were nearly constant, whereas yield strength and hardness values increased slightly. The increase of mechanical properties in slowly sintered alloys with C contents of up to 0.75 wt% is attributed to the increase of lamellar pearlite fraction. The micromechanical modeling of ferrite-pearlite steels clearly demonstrates the effect of pearlite fraction on strength [27].

The slowly sintered alloys with C contents of ≥ 0.75 wt% are grouped in eutectoid and hypereutectoid steels. To give supporting evidence, the eutectoid points of the Fe-1.5Cr-0.2Mo-*x*C system were evaluated from thermal analysis results, as given in Figure 10. The measured eutectoid point is at 765.2°C and 0.77 wt% C. It can be seen that the temperature of the austenite to pearlite transformation decreases rapidly when the carbon content increases up to 0.75% and does not change much above that. Carbon enhances the stability of austenite, thereby reducing the driving force for pearlite formation. The microstructures of eutectoid and hypereutectoid Fe-1.5Cr-0.2Mo-*x*C steels comprise lamellar pearlite as the main component and proeutectoid carbide networks as the minor one.

The slight increase of mechanical properties in slowly cooled sintered alloys with C contents of ≥ 0.75 wt% is attributed to the lamellar pearlite interlamellar spacing value, which decreases with increasing C content (Figure 11). It was previously reported that the interlamellar spacing had Hall-Petch relationship with yield strength and hardness but not with tensile strength and elongation [28].

In fast-cooled sintered alloys tensile strength, yield strength, and hardness values increased with increasing C contents of up to 0.75 wt%. With C contents of > 0.75 wt%, tensile strength and hardness values showed unsystematic change with respect to C content whereas yield strength values increased slightly. According to the microstructural characterization of fast-cooled sintered alloys given above, there are several microstructural factors contributing to the increases in tensile strength, yield strength, and hardness. They include ferrite grain size and morphology, FC mixtures, and MA constituents. Although the fast-cooled sintered alloys have microstructural changes, the tensile strength (Figure 9(a)) and hardness (Figure 9(d)) of these sintered alloys increase with increasing C content.

However, the elongation values of fast-cooled sintered alloys are inferior to those of slowly cooled sintered alloys (Figure 9(d)). This means that all microstructural components, fine ferrite grains, elongated shape plates, MA constituent, FC mixtures (UB and IB), and martensite, in fast-cooled sintered alloys, can have a negative impact on ductility.

The change of coarse equiaxed to fine equiaxed ferrite grains in sintered FC015C alloy leads to the reduction of the elongation value to less than 40% of the value of sintered FC015C alloy. The decreased elongation with decreasing ferrite grain size was previously reported [29].

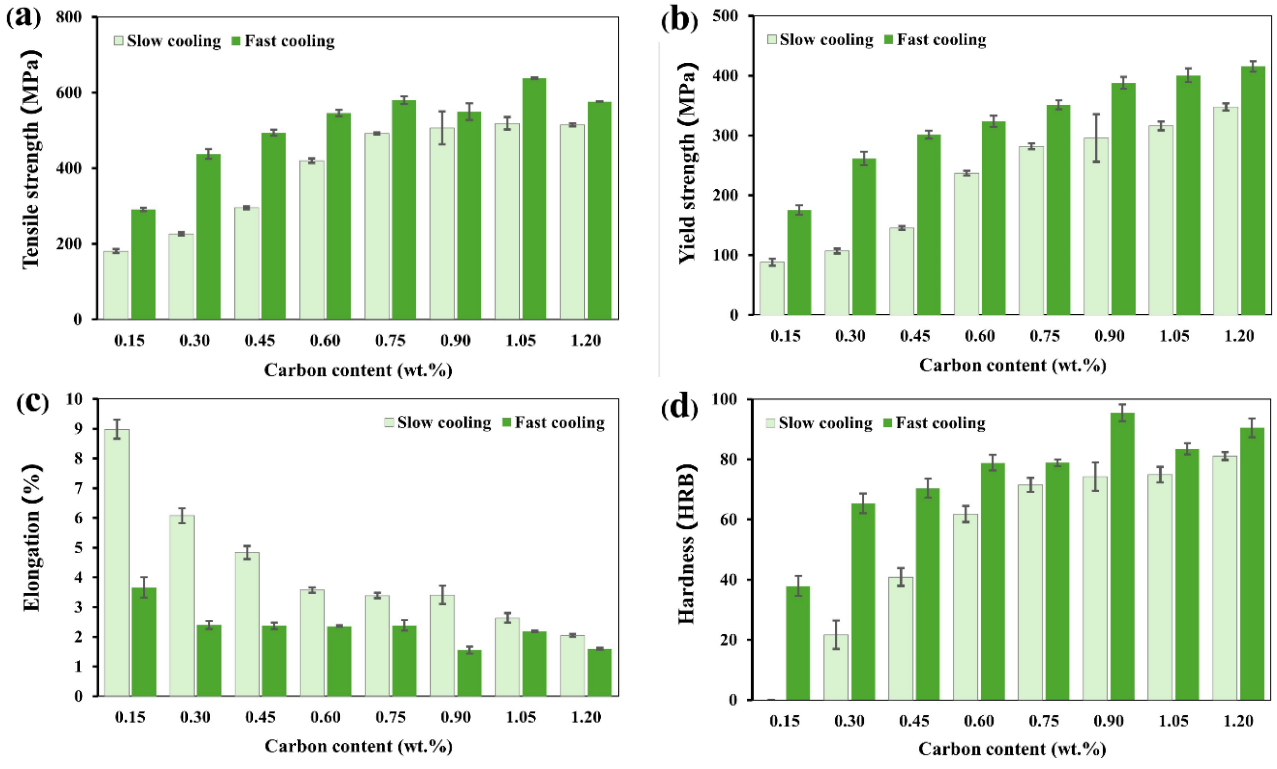

Figure 9. Mechanical properties of sintered alloys; (a) tensile strength, (b) yield strength, (c) elongation, and (d) hardness.

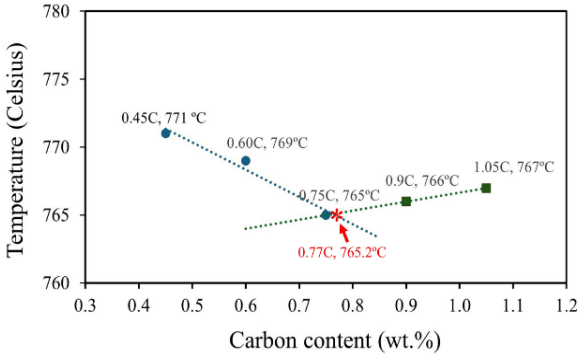

Figure 10. Plots of transformation temperatures, determined by differential scanning calorimetry, against C contents of slowly cooled sintered Fe-1.5Cr-0.2Mo-*x*C alloys.

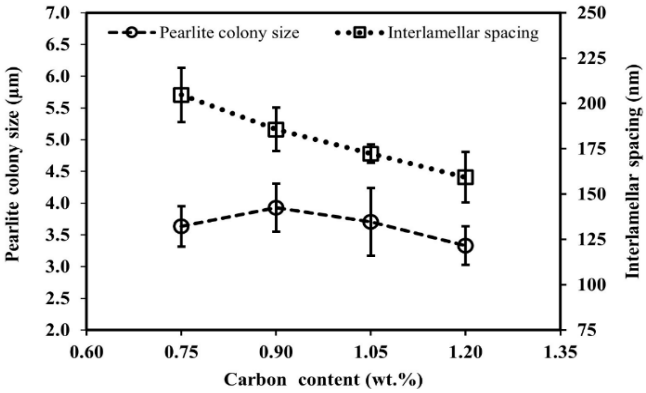

Figure 11. Plots of pearlite colony size and interlamellar spacing of pearlite in sintered alloys with C contents of ≥ 0.75 wt%.

The MA constituent seems to have a negative impact on steel ductility. In general, a remarkable decrease in toughness can be attributed to the volume fraction of the MA constituent [30]. Li *et al.* [31] reported that microcracks easily develop at the interface between MA constituents and matrix once the stress concentration reaches the critical stress of the interface, and they progressively spread to the matrix. The hard phase, such as the MA constituent, is the nucleation of a microcrack, which immediately reaches the boundary of the MA constituents/matrix [32].

In sintered FC060C alloy and FC075C alloy, precipitation of carbide particles on ferrite plate boundaries results in the formation of FC mixtures, and some untransformed austenite regions transform to large MA blocks. The microstructure consisting of dominant FC mixtures and large MA blocks in fast-cooled sintered alloys provides strengthening effect higher than full pearlite structure in slowly cooled sintered alloys

In sintered FC090C alloy, the eutectoid transformation of IB competes with the stability of untransformed austenite regions. The microstructure consisting of a dominant MA matrix with distributed IB units still has an appreciable strengthening effect. The fraction of IB increases significantly in sintered FC105C alloy, leading to high strength and hardness. The formation of IB in sintered alloys under fast cooling was previously reported in fast-cooled sintered Fe-1.50Mo-*x*C alloys with C contents of 1.05 wt% and 1.20 wt% [8] and fast-cooled sintered Fe-0.50Mo- 0.15Mn-2.10Si-0.90C [26] alloys. The strength and hardness of sintered FC120C alloy are lessened due to the presence of thick proeutectoid carbide particles along prior austenite grain boundaries.

The strength and hardness of slowly cooled sintered alloys increase with lamellar pearlite fraction, whereas the elongation decreases with decreasing PF fraction. The presence of proeutectoid carbide particles on grain boundaries of slowly cooled sintered high C alloys also causes elongation reduction. The increase of strength and hardness of fast-cooled sintered alloys is attributed to several factors, such as fine PF grains, acicular microstructural components (ferrite plates and MA constituents), MA constituent fraction, and IB fraction. The elongation values of fast-cooled sintered alloys with all investigated C contents are inferior to those of slowly cooled sintered alloys with the same C contents. The inferior ductility reflects the strength-ductility trade-off commonly found in conventional steels. Although austenite coexists with martensite as MA constituents, the transformation-induced plasticity (TRIP) effect is not observed in most fast-cooled sintered alloys.

4. Conclusions

Microstructural development in sintered Fe-1.5Cr-0.2Mo-*x*C alloys, produced under different cooling rates of 0.1°C·s^{-1} and 5.4°C·s^{-1} was investigated. Slowly sintered Fe-1.5Cr-0.2Mo-*x*C alloys exhibited microstructural change from hypoeutectoid to eutectoid and to hypereutectoid steel microstructural features with increasing carbon content. The experimentally determined eutectoid point was at 765.2°C and 0.77 wt% C. The fast-cooling rate of 5.4°C·s^{-1}caused microstructural changes depending on carbon content. The change involved the competition between the formation of the FC mixture and that of the MA constituent. The increase of tensile strength of slowly cooled sintered Fe-1.5Cr-0.2Mo-*x*C alloys with increasing carbon content was attributed to the increase of pearlite fraction while the increase of tensile strength of fast cooled sintered Fe-1.5Cr-0.2Mo-*x*C alloys was attributed to ferrite morphology change the formation of FC mixture and the formation of MA constituent.

Acknowledgements

The authors would like to thank all supports for this work, which is financially supported via the project ‘Design and manufacturing of replacement parts for railway applications ‘(P1951261)’ under NSTDA, Pathum Thani, Thailand. Technical supports are obtained from National Metal and Materials Technology Center (MTEC), Pathum Thani, Thailand. Thanks to the Department of Industrial Physics and Medical Instrumentation (IMI) of King Mongkut’s University of Technology North Bangkok.

References

[1] H. Okamoto, "The C-Fe (carbon-iron) system," *Journal of Phase Equilibria and Diffusion*, vol. 13, p. 543-565, 2007.

[2] G. Miyamoto, Y. Karube, and T. Furuhara, "Formation of grain boundary ferrite in eutectoid and hypereutectoid pearlitic steels," *Acta Materialia*, vol. 103, p. 370-381, 2016.

[3] S. Chen, L. Li, Z. Peng, X. Huo, and H. Sun, "On the correlation among continuous cooling transformations, interphase precipitation and strengthening mechanism in Ti-microalloyed steel," *Journal*

of Materials Research and Technology, vol. 10, p. 580-593, 2021.

[4] P. J. de Castro, A. C. de F. Silveira, T. M. Ivaniski, C. J. Turra, J. Epp, and A. da S. Rocha, "Two-step continuous cooling heat treatment applied in a low carbon bainitic steel," *Materials Research*, vol. 24, p. e20200334, 2021.

[5] K. F. Rodrigues, and G. L. de Faria, "Characterization and prediction of continuous cooling transformations in rail steel," *Materials Research*, vol. 24, p. e20200519, 2021.

[6] J. C. Zhao, and M. R. Notis, "Continuous cooling transformation kinetics versus isothermal transformation kinetics of steels: a phenomenological rationalization of experimental observations," *Materials Science and Engineering: R: Reports*, vol. 15, no. 4-5, pp. 135-207, 1995.

[7] W. Srijampan, A. Wiengmoon, A. Wanalerkngam, S. Boonmee, Y. Thanyaporn, N. Tosangthum, and R Tongsri, "Identification of carbides and phase transformations in sintered Fe-Mo-Mn-C alloys produced under a slow continuous cooling," *ISIJ International*, vol. 62, no. 11, pp. 2366-2373, 2022.

[8] A. Wanalerkngam, S. Boonmee, T. Srichumpong, M. Morakotjinda, N. Tosangthum, R. Tongsri, "Influences of cooling rate and carbon content on microstructure and mechanical properties of sintered Fe-1.5Mo-xC alloys," *IOP Conference Series: Materials Science and Engineering*, vol. 1137, p. 012033, 2021.

[9] W. Koetniyom, P. Chantawet, N. Tosangthum, M. Morakotjinda, T. Yotkaew, P. Wila, and R. Tongsri, "Effect of carbon addition on microstructure and properties of boron-containing steel sintered under different atmospheres," *Journal of Metals, Materials and Minerals*, vol.29, no.1, pp.22-30, 2019.

[10] I. Howe, "Lean sinter materials point way towards greater profitability," *Metal Powder Report*, vol. 63, p. 32-34, 2008.

[11] L. Čiripová, E. Hryha, E. Dudrová, and A. Výrostková, "Prediction of mechanical properties of Fe-Cr-Mo sintered steel in relationship with microstructure," *Materials and Design*, vol. 35, pp. 619-625, 2012.

[12] M. Hebda, S. Gądek, K. Miernik, and J. Kazior, "Effect of the cooling rate on the phase transformation of Astaloy CrL powders modified with SiC addition," *Advanced Powder Technology*, vol. 25, pp. 543-550, 2014.

[13] Y. Ohmori, A. T. Davenport, and R. W. K. Honeycombe, "Crystallography of pearlite," *Transactions of the Iron and Steel Institute of Japan*, vol. 12, pp. 128-137, 1972.

[14] W. T. Reynolds, H. I. Aaronson, and G. Spanos, "A summary of the present diffusionist views on bainite," *Materials Transactions, JIM*, vol. 32, pp. 737-746, 1991.

[15] P. Cizek, B. P. Wynne, C. H. J. Davies, B. C. Muddle, and P. D. Hodgson, "Effect of composition and austenite deformation on the transformation characteristics of low-carbon and ultralow-carbon microalloyed steels," *Metallurgical and Materials Transactions A*, vol. 33, pp. 1331-1349, 2002.

[16] S. Zajac, V. Schwinn, and K. H. Tacke, "Characterisation and quantification of complex bainitic microstructures in high and ultra-high strength linepipe steels," *Materials Science Forum*, vol. 500-501, pp. 387-394, 2005.

[17] L. Lan, M. Yu, and C. Qiu, "On the local mechanical properties of isothermally transformed bainite in low carbon steel," *Materials Science and Engineering A*, vol. 742, pp. 442-450, 2019.

[18] K. Sheikhi Moghaddam, M. Ghambari, H. Farhangi, and N. Solimanjad, "Effect of sinter hardening on microstructure and mechanical properties of Astaloy 85Mo," *Journal of Iron and Steel Research, International*, vol. 19, pp. 43-46, 2010.

[19] J. Yin, M.Hillert, and A. Borgenstam, "Second stage of upper bainite in a 0.3 mass pct C steel," *Metallurgical and Materials Transactions A*, vol. 48, pp. 1444-1458, 2017.

[20] M. Perez, and A. Deschamps, "Microscopic modelling of simultaneous two-phase precipitation: application to carbide precipitation in low-carbon steels," *Materials Science and Engineering A*, vol. 360, pp. 214-219, 2003.

[21] M. C. Zhao, K. Yang, Y. Shan, "The effects of thermo-mechanical control process on microstructures and mechanical properties of a commercial pipeline steel," *Materials Science and Engineering A*, vol. 335, pp. 14-20, 2002.

[22] Z. Moreno-Fabian, and G.Solís-Bravo, "Effects of cooling media on the formation of martensite-austenite microconstituent in a HSLA steel," *Revista de Metalurgia*, vol. 58, article e214, 2022.

[23] R. Kannan, Y. Wang, and L. Li, "A thermodynamic study of inverse bainitic transformation," *Journal of Materials Science*, vol. 53, pp. 12583-12603, 2018.

[24] K. R. Kinsman, and H. I. Aaronson, "The inverse bainite reaction in hypereutectoid Fe-C alloys," *Metallurgical Transactions*, vol. 1, pp. 1485-1488, 1970.

[25] A. Borgenstam, P. Hedström, M. Hillert, P. Kolmskog, A. Stormvinter, and J. Ågren, "On the symmetry among the diffusional transformation products of austenite," *Metallurgical and Materials Transactions A*, vol. 42, pp. 1558-1574, 2011.

[26] W. Srijampan, A. Wiengmoon, P. Nakornkaew, T. Patcharawit, T. Yotkaew, N. Tosangthum, R. Tongsri, "Effects of silicon carbide contents on the microstructure of sintered steel," *ScienceAsia*, vol. 47S, pp. 51-59, 2021.

[27] N. Ishikawa, D. M. Parks, S. Socrate, and M. Kurihara, "Micro-mechanical modeling of ferrite-pearlite steels using finite element unit cell models," *ISIJ International*, vol. 40, pp. 1170-1179, 2000.

[28] O. P. Modi, N. Desmukh, D. P. Mondal, A. K. Jha, A. H. Yegneswaran, and H. K. Khaira, "Effect of interlamellar spacing on the mechanical properties of 0.65% C steel," *Materials Characterization*, vol. 46, pp. 347-352, 2001.

[29] R. Song, D. Ponge, D. Raabe, J. G. Speer, and D. K. Matlock, "Overview of processing, microstructure and mechanical properties of ultrafine-grained bcc steels," *Materials Science and Engineering A*, vol. 441, pp. 1-17, 2006.

[30] Y. Shi, and Z. Han, "Effect of weld thermal cycle on microstructure and fracture toughness of simulated heat-affected zone for an 800 MPa grade high strength low alloy steel," *Journal of Materials Processing Technology*, vol. 207, pp. 30-39, 2008.

[31] Y. Li, and T.N. Baker, "Effect of morphology of martensite-austenite phase on fracture of weld heat affected zone in vanadium

and niobium microalloyed steels," *Materials Science and Technology*, vol. 26, pp. 1029-1040, 2010.

[32] C. Qiu, L. Lan, D. Zhao, X. Gao, and L. Du, "Microstructural evolution and toughness in the HAZ of submerged arc welded low welding crack susceptibility steel," *Acta Metallurgica Sinica (English Letters)*, vol. 26, pp. 49-55, 2013.